EFFECT OF RADIATIVE TRANSFER CODES FOR MINERAL MAPPING USING HYPERSPECTRAL DATA

Karl STAENZ[1], Christian NADEAU[2], Robert A. NEVILLE[1], and Jeff SECKER[1]

[1]Canada Centre for Remote Sensing,
588 Booth Street, Ottawa, Ontario, Canada K1A 0Y7
[2]MacDonald Dettwiler and Associates,
13800 Commerce Parkway, Richmond, B.C., Canada V6V 2J3

ABSTRACT *– The study presented in this paper investigated the influence of radiative transfer (RT) codes upon the surface reflectance retrieval and, ultimately, upon the spectral unmixing for mineral identification and mapping of mineral abundances. The effect of post-processing of the RT code retrieved surface reflectance was also studied. For this purpose, an AVIRIS radiance cube acquired over the Cuprite mining district area in Nevada on June 12, 1996 was used to generate the surface reflectance using the three RT codes ATREM (ATmospheric REMoval program), CAM5S (Canadian Advanced Modified 5S), and MODTRAN4 (MODerate atmospheric radiance and TRANsmittance model). The mineral abundance maps generated from MODTRAN4 reflectance data showed the best match with a classification carried out by the United States Geological Survey [USGS 98]. However, the resulting fraction maps produced based on ATREM and CAM5S reflectance data are quite similar for most minerals identified, with the exception of montmorillonite and chalcedony. In addition, differences occur in several cases between the RT code retrieved reflectance and post-processed data.*

1 - INTRODUCTION

Identification and subsequent mapping of minerals has become possible with hyperspectral data [Clark 90; Boardman 96; Cloutis 96]. Several processing steps such as surface reflectance retrieval, endmember selection, and spectral unmixing, are applied to such data to produce mineral abundance maps. A significant step in the data processing chain is the retrieval of surface reflectance. In order to calculate surface reflectance from remotely measured radiance, radiative transfer (RT) codes play an important role for removing the atmospheric scattering and gaseous absorption effects [Gao 93; Richter 96; Staenz 97a]. Given the complexity of hyperspectral data, the surface reflectance retrieval results depend strongly on the selected RT code as well as on the radiometric and spectral calibration of the sensor [Staenz 00; Secker 00].

This paper concentrates on the assessment of mineral abundance maps generated from surface reflectances using the three atmospheric RT codes CAM5S (Canadian Advanced Modified 5S; O'Neill 96), ATREM (ATmospheric REMoval program; Gao 93; CIRES 99), and MODTRAN4 (MODerate atmospheric radiance and TRANsmittance model; Berk 89 and 98). For this purpose, Airborne Visible/Infrared Imaging Spectrometer (AVIRIS) data from the Cuprite mining district of Nevada were processed to yield abundances (fractions) of minerals. These fraction images were compared quantitatively against a reference to demonstrate the effect of the different RT codes on the unmixing results. The main portion of the analysis was carried out on the Imaging Spectrometer Data Analysis System (ISDAS), an advanced hyperspectral analysis software package developed at the Canada Centre for Remote Sensing [Staenz 98].

2 - STUDY SITE AND DATA DESCRIPTION

The site selected for this study lies within the Cuprite mining district of Nevada (37.6^0 N and 117.2^0 W). This site has been used as a test area for mineral mapping in hyperspectral remote sensing for a many years [Goetz 85; Hook 90; Swayze 92; Neville 98]. Accordingly, this site is very well characterized in terms of mineralogy. This and the excellent exposure of alteration minerals such as alunite, calcite, kaolinite, buddingtonite, silica, and others. together with limited soil development and sparse vegetation make this area an ideal test site for evaluation of hyperspectral mineral mapping capabilities.

One of the Cuprite standard AVIRIS data sets available form NASA's Jet Propulsion Laboratory (JPL) has been used for this study. This particular data cube was collected on June 12, 1996. AVIRIS acquires imagery at approximately 20 m ground resolution in 224 spectral bands, each about 10 nm wide, in the 400-nm to 2500-nm wavelength range. Additional information for validation purposes include reference data sets consisting of a detailed mineral map retrieved from AVIRIS 1998 data by [USGS 98] and ground spectra acquired with GER3700™ and PIMA™ spectroradiometers.

3 - APPROACH

3.1 Surface Reflectance Retrieval

Prior to surface reflectance retrieval, an assessment of noise was carried out in the principal component (PC) domain. The results revealed that no significant noise pattern could be found. In addition, no significant errors were found in the wavelength position of the AVIRIS bands. It should be noted that the bands in the strong water absorption regions around 1380 nm and 1870 nm were not included in the analysis.

The RT codes used to remove scattering and gaseous effects are ATREM, CAM5S, and MODTRAN4. These codes are models commonly used in hyperspectral remote sensing to retrieve surface reflectances from at-sensor radiances. The specific features of these models are summarized in [Staenz 00]. ATREM was used outside of ISDAS in its original configuration as available from the University of Colorado [CIRES 99] while MODTRAN4 and CAM5S were run inside ISDAS as part of a look-up table (LUT) procedure.

The MODTRAN/CAM5S procedure is based on a LUT approach with tunable breakpoints as described in [Staenz 97a], to reduce significantly the number of radiative RT code runs. A selected RT code was used in forward mode to generate the radiance LUTs, one for each of a 5% and 60% flat reflectance spectrum. These LUTs were produced for five pixel locations equally spaced across the swath, including nadir and swath edges, for a range of water vapour contents, and for single values of aerosol optical depth (horizontal visibility) and terrain elevation. The specification of these parameters and others required for input into the RT codes are listed in Table 1. The finest available wavelength grid intervals were used for the RT code runs. None of the BRDF options available in CAM5S and MODTRAN4 were used for this study. It should be noted that a common user interface is used for the specification of the atmospheric conditions.

For the retrieval of the surface reflectance, the LUTs were adjusted only for the pixel location in the swath and water vapour content using a bi-linear interpolation routine [Press 92] since single values for the other LUT parameters were used for the entire cube. For this purpose, the water vapour content was estimated for each pixel in the scene with an iterative curve fitting technique [Staenz 97b]. The surface reflectance was then computed for each pixel as described in [Staenz 97a].

The next step of processing performs an empirical correction for irregularities in the reflectance data (band-to-band errors) that may have originated in the sensor, or that may have resulted from the approximation made in atmospheric modelling and the selection of RT code input parameters. These band-to-band errors were removed by calculating correction gains and offset using spectrally flat targets [Staenz 99]. The removal of these errors is referred to in the following sections of this paper as post-processing.

Table 1: Input parameters for radiative transfer code runs.

Radiative Transfer Code	**ATREM**	**CAM5S**	**MODTRAN4**
Atmospheric model	US standard 62	US standard 62	US standard 76
Aerosol model	Continental	Desert	Desert
Date of overflight	June 12, 1996	June 12, 1996	June 12, 1996
Solar zenith angle	15.8°	15.8°	15.8°
Solar azimuth angle	153.7°	153.7°	153.7°
Sensor zenith angle	Fixed	Variable	Variable
Sensor azimuth angle	Fixed	Variable	Variable
Terrain elevation (above sea level)	1.524 km	1.524 km	1.524 km
Sensor altitude (above sea level)	20.100 km	20.100 km	20.100 km
Water vapour content	variable	variable	variable
Ozone column	as per model	as per model	as per model
CO_2 mixing ratio	as per model	as per model	300 ppm
Horizontal visibility	50 km	50 km	50 km
Wavelength grid interval	2.5 nm	10 cm^{-1}	1 cm^{-1}

3.2 Endmember Selection and Spectral Unmixing

Endmembers needed for the spectral unmixing were selected from the data cube itself using an automated method. This method is called Iterative Error Analysis (IEA) and is described in detail by [Szeredi 00]. To start, the average spectrum of the scene is used to unmix the data set. When a data set is unmixed, a residual error image is produced. These errors are calculated using a least-square estimate between the average spectrum and the spectrum of each pixel. The errors are also a measure of the distance in N-dimensional space (N = number of bands) between the average spectrum and all the spectra of the data set. The next step is to find the pixel or pixels that encompass the largest errors, i.e., that are furthest away from the average spectrum. The user provides the number of pixels forming these endmembers. This first endmember is then used to unmix the image cube, and the average spectrum is discarded. The errors will again be used to find the furthest pixels from the first endmember and will create the second endmember. This process is repeated until the number of endmembers predetermined by the user is reached. In this case, 30 endmembers have been selected.

Once all the endmembers were found, the image cube was unmixed using a constrained linear technique [Shimabukuru 91; Boardman 95]. Spectral unmixing uses a linear combination of a set of endmember spectra to unmix the composite spectrum into endmember fractions (between 0 and 1) for each pixel of the scene. The full wavelength range of the AVIRIS sensor was utilised for the endmember selection and spectral unmixing.

In a final step, the resulting fraction maps were compared with each other on a quantitative basis

using the Average Euclidean Distance Coefficient (AEDC) [Romesburg 84]:

$$AEDC = \sqrt{\frac{\sum_{i=1}^{n}(x_i - y_i)^2}{n}},$$

(3.2.1)

where x_i is the reference fraction of pixel i, y_i is the fraction to be compared of pixel i, and n is the total number of pixels of the fraction map. AEDC provides a measure for the deviation from the y = x line. Accordingly, AEDC = 0 means a perfect match between the reference fraction map and the fraction map to be compared.

4 – RESULTS

4.1 Surface Reflectance Retrieval

The surface reflectance retrieved with the different RT codes indicates that the gas absorption regions are the major areas of concern as illustrated in Fig. 1 for the endmember spectra of alunite.

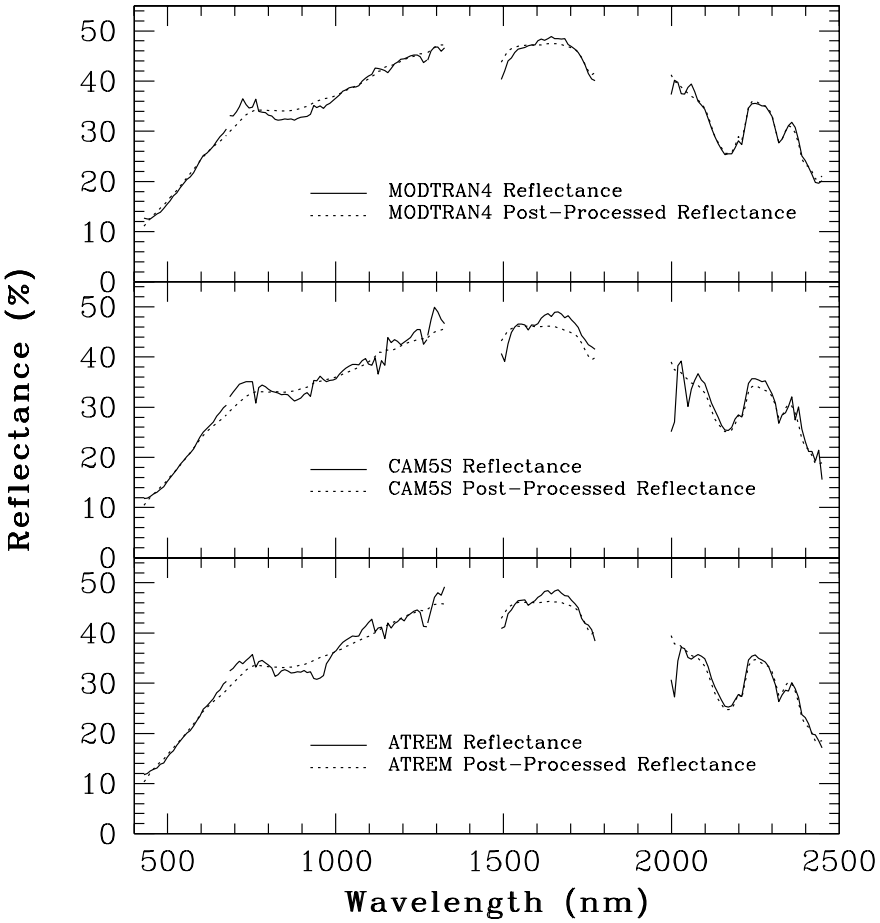

Fig. 1: Alunite endmember surface reflectance spectra retrieved with MODTRAN4 (top), CAM5S (centre), and ATREM (bottom) from the

Cuprite AVIRIS cube in comparison with associated post-processed spectra. The spectra were generated from 10 to 13 pixels.

The reflectance is especially affected in the 940-nm and the 1130-nm water absorption bands, as well as in the wings of the strong 1380-nm and 1870-nm water absorption regions. Problems were also encountered in the O_2 absorption regions, especially in the 760-nm absorption feature and to some extent in the 1265-nm region for all three codes. The same is valid for the CO_2 region at 2055 nm for CAM5S and to a lesser degree for ATREM and MODTRAN4. These differences are mainly due to the use of different transmittance models and wavelength grid intervals in these RT codes. Line wing absorption effects are accounted for in the calculation of the transmittance in MODTRAN4, but not in ATREM and CAM5S. Significant differences occur also in the 2100-nm to 2450-nm region between the retrieved reflectances. These differences are mostly due to the different solar exo-atmospheric irradiance functions used in the RT codes [Staenz 95]. These functions are based on [Neckel 84] and [Green 93] for ATREM, [Iqbal 83] for CAM5S, and [Kurucz 94] for the MODTRAN4 run.

Based on these results, MODTRAN4 outperforms ATREM and CAM5S. Such a performance of these RT codes was previously reported in a study which indicates an average relative error between retrieved and ground-based reflectance of 2.0 % for MODTRAN4, 3.2 % for ATREM and 3.7 % for CAM5S [Staenz 00].

4.2 Endmember Selection and Identification

Tabel 2 lists the minerals identified on the basis of the 30 extracted endmembers. These endmembers were compared with lab spectra [Grove 92] and particularly the absorption features located mainly in the 2000-nm to 2500-nm wavelength region. Subsequently, they were grouped into single mineral categories wherever possible. An exception is the category alunite/kaolinite which probably represents an intimate mixture between these two minerals. Also a relatively high number of endmembers could not be categorized. Despite this fact, a comparison with the [USGS 98] mineral list from the same area shows good agreement. Table 2 indicates that for each of the data sets at least one endmember could be associated with one of the mineral categories, with the exception of chalcedony for the ATREM post-processed data cube. In most cases more than one endmember could be identified per mineral category. This is mainly due to the different degree of contamination with other minerals (e.g., muscovite), structural differences (e.g., kaolinite), and elemental substitution. The combination of illumination and terrain (slope and aspect: bidirectional reflectance distribution factor effect) also affects the number of endmembers selected by the IAE technique for a particular mineral category. The different number of endmembers extracted from the data sets for a specific mineral category does not necessarily mean that the mapped areas differ

Table 2: Endmembers identified. The numbers in the table indicate the number of endmembers found per mineral type. (Ref = original reflectance data, PP = post-processed reflectance data).

Endmember	**MODTRAN4**		**ATREM**		**CAM5S**	
	Ref	PP	Ref	PP	Ref	PP
Chalcedony (opal)	2	1	4	0	3	1
Alunite	2	2	2	2	2	2
Kaolinite	3	3	3	3	3	3
Alunite/Kaolinite Mixture	7	6	6	6	6	6
Montmorillonite	2	1	1	1	1	1
Dickite	1	2	1	2	2	1
Muscovite	4	4	4	4	5	4

Buddingtonite	1	1	1	1	1	1
Calcite	1	1	1	1	1	1
Unknown	7	9	7	10	6	10

significantly in size. This is true as long as the specific mineral is spectrally well characterized.

The lack of proper removal of atmospheric absorption features can cause problems for the identification of a specific mineral. This is especially a problem when these absorption regions are on top of the mineral absorption features. For example, one of two the montmorillonite endmembers could be identified only using the MODTRAN4 reflectance data cube. In this case, this mineral could not be mapped properly, according to the [USGS 98] map, for the other data cubes with just one endmember. With the exception of dickite (MODTRAN4 and ATREM), more endmembers could be identified using the original reflectance data than the post-processed ones. This is due to the post-processing effect that can cause a smoothing of weak, but important absorption features for mineral identification.

4.3 Spectral Unmixing

The fraction maps of the individual mineral categories extracted from the MODTRAN4 reflectance data, were selected as references for comparisons of the fraction maps on a pixel basis. The choice is based on the good agreement between these MODTRAN4 fraction maps and the classification reported by [USGS 98]. The results are summarized in Table 3. In general, a fairly good match was achieved for most minerals, especially for buddingtonite and kaolinite. Exceptions are the minerals montmorillonite and chalcedony, and as well to a lesser degree, the alunite/kaolinite mixture. For these minerals, the areas of occurrences do not coincide; see for example the montmorillonite maps in Fig. 2. The reason for the montmorillonite case is that one of the montmorillonite endmembers was identified as chalcedony for the ATREM and CAM5S cases, as well as for the MODTRAN4 post-processed data. The difference between the fraction maps extracted from the original reflectance and post-processed data is similar in most cases. An exception is montmorillonite and chalcedony for the MODTRAN4 case as well as dickite for the ATREM and CAM5S cases.

Table 3: Correlation expressed via the AEDC between the retrieved fraction maps. **(**Ref = original reflectance data, PP = post-processed reflectance data, N/A = no endmember identified).

Endmember	**MODTRAN4**		**ATREM**		**CAM5S**	
	Ref	PP	Ref	PP	Ref	PP
Chalcedony (opal**)**	-	0.045	0.151	N/A	0.147	0.066
Alunite	-	0.015	0.015	0.016	0.015	0.017
Kaolinite	-	0.008	0.010	0.010	0.010	0.009
Alunite/Kaolinite Mixture	-	0.044	0.053	0.063	0.053	0.050
Montmorillonite	-	0.170	0.170	0.172	0.170	0.172
Dickite	-	0.019	0.009	0.018	0.020	0.008
Muscovite	-	0.041	0.039	0.039	0.040	0.038
Buddingtonite	-	0.005	0.007	0.006	0.006	0.005
Calcite	-	0.020	0.019	0.022	0.021	0.024

5 - CONCLUSIONS

The effect of different RT codes for mineral mapping was studied in this paper. For this purpose, the RT codes ATREM, CAM5S, and MODTRAN4 were applied to AVIRIS radiance data of Cuprite, Nevada to retrieve surface reflectance. Subsequently, 30 endmembers were selected from

the reflectance data and grouped into nine minerals and one unknown category. Endmembers could be identified with the exception of chalcedony (CAM5S, post-processed) for each of the mineral categories although the number of endmembers vary depending on the RT codes used and whether

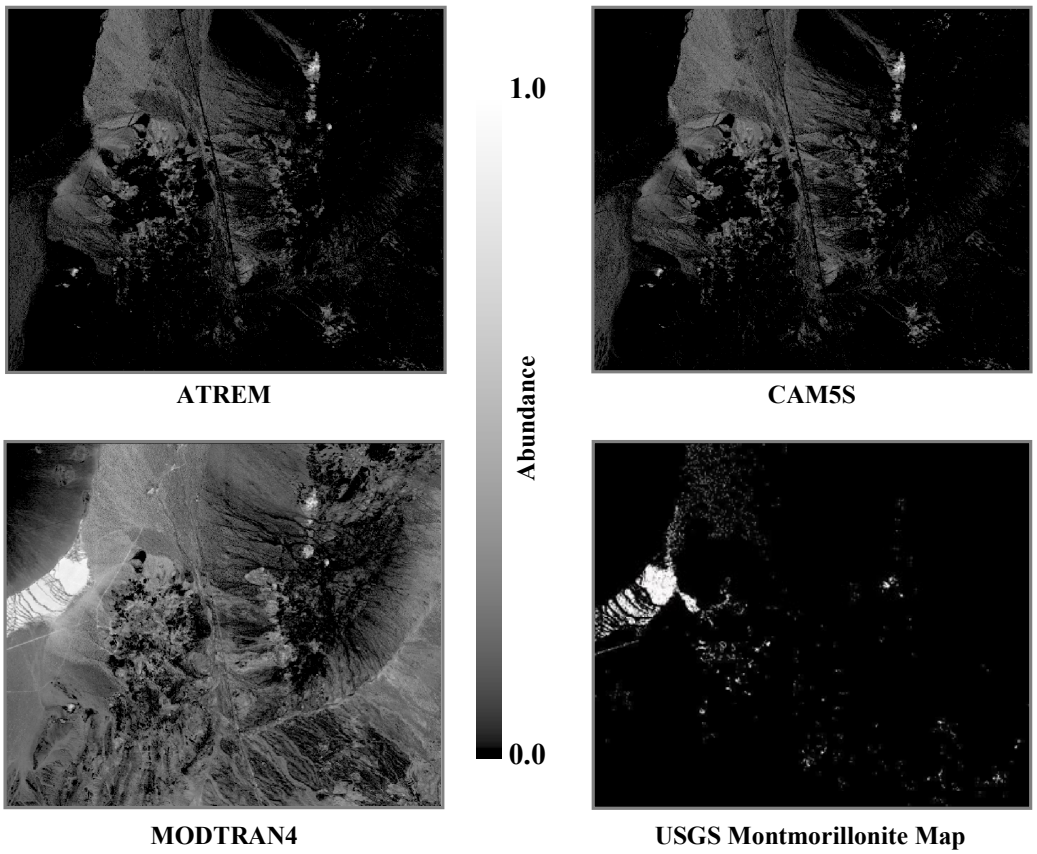

Fig. 2: Distribution of montmorillonite abundance (fraction) based on ATREM, CAM5S, and MODTRAN4 retrieved reflectance data. The [USGS 98] montmorillonite map is shown as reference.

the data was post-processed or not. Fewer endmembers could be associated with minerals for the post-processed data cubes. A comparison of the mineral fraction maps generated with constrained linear spectral unmixing revealed differences in some cases depending on the RT code used and post-processing. Significant differences occurred for the minerals montmorillonite and chalcedony for the MODTRAN4 retrieved data compared to the other cases. The ATREM and CAM5S cases produce generally similar fraction maps, although some differences occur in some cases between the RT-code retrieved and post-processed data. In general, MODTRAN4 retrieved reflectance data yielded fraction maps that show the best match with a mineral classification carried out by [USGS 98] over the same area using AVIRIS data.

6 – ACKNOWLEDGEMENTS

The authors like to thank the Jet Propulsion Laboratory for making the AVIRIS data available to us.

7 - REFERENCES

[Berk 89] A. Berk, L.S. Bernstein, and D.C. Robertson: "MODTRAN: A Moderate Resolution Model for LOWTRAN7", *Final Report, GL-TR-0122*, AFGL, Hanscom AFB, Maryland, U.S.A., 1989, 93 pages.

[Berk 98] A. Berk, L.S. Bernstein, G.P. Anderson, P.K. Acharya, D.D. Robertson, J.H. Chetwynd, and S.M. Adler-Golden: "MODTRAN Cloud and Multiple Scattering Upgrades with Application to AVIRIS", *Remote Sensing of Environment*, 1998, Vol. 65, pp. 367-375.

[Boardman 95] J.W. Boardman: "Analysis, Understanding and Visualization of Hyperspectral Data as Convex Sets in n-Space", *Proceedings of the International SPIE Symposium on Imaging Spectrometry*, Orlando, Florida, U.S.A., 1995, SPIE Vol. 2480, pp. 23-36.

[Boardman 96] J.W. Boardman, and J.F. Huntington: "Mineral Mapping with 1995 AVIRIS Data", *Summaries of the Sixth Annual JPL Airborne Earth Science Workshop*, Pasadena, California, U.S.A., 1996, JPL-Publication 96-4, Vol. 1, pp. 9-11.

[Clark 90] R.N. Clark, T.V.V. King, M. Klejwa, G.A. Swayze, and N. Vegro: "High Spectral Resolution Reflectance Spectroscopy of Minerals", *Journal of Geophysical Research*, 1990, Vol. 95, pp. 12653-12680.

[CIRES 99] CIRES: "Atmosphere REMoval Program (ATREM)", *User's Guide, Version 3.1*, Center for the Study from Space, Cooperative Institute for Research in Environmental Sciences (CIRES), University of Colorado, Boulder, Colorado, U.S.A., 1999, 36 pages.

[Cloutis 96] E.A. Cloutis: "Hyperspectral Geological Remote Sensing Evaluation and of Analytical Techniques", *International Journal of Remote Sensing*, 1996, Vol. 17, No. 12, pp. 2215-2242.

[Gao 93] B.-C. Gao, K.B. Heidebrecht, and A.F.H. Goetz: "Derivation of Scaled Surface Reflectances From AVIRIS Data", *Remote Sensing of Environment*, 1993, Vol. 44, pp. 165-178.

[Goetz 85] A.F.H. Goetz, and V. Srivastava: "Mineralogic Mapping in the Cuprite Mining District, Nevada", *Proceedings of the First AIS Workshop,* Pasadena, California, U.S.A., 1985, JPL-Publication 85-41, pp. 22-31.

[Green 93] R.O. Green, and B.-C. Gao: "A Proposed Update to the Solar Irradiance Spectrum Used in LOWTRAN and MODTRAN", *Summaries of the Fourth Annual JPL Airborne Geoscience Workshop,* Washington, D.C., 1993, JPL-Publication 93-26, Vol. 1, pp. 81-84.

[Grove 92] C.I. Grove, S.J. Hook, and E.D. Paylor II: "Laboratory Reflectance Spectra of 160 Minerals, 0.4 to 2.5 Micrometers", Pasadena, California, U.S.A., 1992, JPL Publication 92-2, 380 pages.

[Hook 90] S.J. Hook, and M. Rast: "Mineralogic Mapping Using Airborne Visible Infrared Imaging Spectrometer (AVIRIS) Shortwave Infrared (SWIR) Data Acquired over Cuprite, Nevada", *Proceedings of the Second Airborne Visible/Infrared*

Imaging Spectrometer (AVIRIS) Workshop, Pasadena, California, U.S.A., 1990, JPL Publication 90-54, pp. 199-207.

[Iqbal 83] M. Iqbal: "An Introduction to Solar Radiation", *Academic Press,* New York, New York, U.S.A., 1983, 390 pages.

[Kurucz 94] R.L. Kurucz: "The Solar Irradiance by Computation", *Proceedings of the 17th Annual Review Conference on Atmospheric Transmission Models,* Geophysics Directorate/Phillips Laboratory, Hanscom AFB, Maryland, U.S.A., 1994, pp.132-141.

[Neckel 84] H. Neckel, and D. Labs: "The Solar Radiation between 3300 and 12500 Angstrom", *Solar Physics,* 1984, Vol. 90, pp. 205-258.

[Neville 98] R.A. Neville, C. Nadeau, J. Lévesque, T. Szeredi, K. Staenz, P. Hauff, and G.A. Borstad: "Hyperspectral Imagery for Mineral Exploration: Comparison of Data from Two Airborne Sensors", *Proceedings of the International SPIE Conference on Imaging Spectrometry IV*, San Diego, California, U.S.A., 1998, pp. 74-83.

[O'Neil 96] N.T. O'Neill, A. Royer, and M.N. Nguyen: "Canadian Advanced Modified 5S (CAM5S)", *Internal Report*, CARTEL-1996-0202, Centre d'applications et de recherches en télédétection (CARTEL), Université de Sherbrooke, Sherbrooke, Québec, Canada, 1996, 46 pages.

[Press 92] Press, W.H., S.A. Teukolsky, W.T. Vetterling, and B.P. Flannery: "Numerical Recipes in C", *Cambridge University Press*, Cambridge, England, 1992, pp. 123-125.

[Richter 96] R. Richter: "Atmospheric Correction of DAIS Hyperspectral Image Data", *Computer & Geoscience*, 1996, Vol. 2, No. 7, pp. 785-793.

[Romesburg 84] H.C. Romesburg: "Cluster Analysis for Researchers", Lifetime Publications, Belmont, California, U.S.A., 1984, 334 pages.

[Secker 00] J. Secker, K. Staenz, R.P. Gauthier, and P. Budkewitsch: "Vicarious Calibration of Airborne Hyperspectral Sensors in Operational Environments", *Remote Sensing of Environment*, 2000 (in press).

[Shimabukuru 91] Y.E. Shimabukuru, and J.A. Smith: "The Least Squares Mixing Models to Generate Fraction Images Derived From Remote Sensing on Multispectral Data*", IEEE Transactions on Geoscience and Remote Sensing*, 1991, Vol. 29, pp. 16-20.

[Staenz 95] K. Staenz, D.J. Williams, G. Fedosejevs, and P.M. Teillet: "Impact of Differences in the Solar Irradiance Spectrum on Surface Reflectance Retrieval with Different Radiative Transfer Codes", *Summaries of the Fifth Annual JPL Airborne Earth Science Workshop,* Pasadena, California, U.S.A., 1995, JPL-Publication 95-1, Vol. 1, pp.153-156.

[Staenz 97a] K. Staenz, and D.J. Williams: "Retrieval of Surface Reflectance from Hyperspectral Data Using a Look-Up Table Approach", *Canadian Journal of Remote Sensing*, 1997, Vol. 23, No. 354-368.

[Staenz 97b] K. Staenz, T. Szeredi, R.J. Brown, H. McNairn, and R. VanAcker: "Hyperspectral Information Extraction Techniques Applied to Agricultural *casi* Data for Detection of Within-Field Variations", *Proceedings of the International Symposium in the Era of Radarsat and the Nineteenth Canadian Symposium on Remote Sensing*, Ottawa, Ontario, Canada, 1997, 8 pages (CD-ROM).

[Staenz 98] K. Staenz, T. Szeredi, and J. Schwarz: "ISDAS - A System for Processing/Analyzing Hyperspectral Data*", Canadian Journal of Remote Sensing*, 1998, Vol. 24, No. 2, pp. 99-113.

[Staenz 99] K. Staenz, R.A. Neville, J. Lévesque, T. Szeredi, V. Singhroy, G.A. Borstad, and P. Hauff: "Evaluation of *casi* and SFSI Hyperspectral Data for Environmental and Geological Applications – Two Case Studies", *Canadian Journal of Remote Sensing*, 1999, Vol. 25, No. 3, pp. 311- 322.

[Staenz 00] K. Staenz, J. Secker, B.-C. Gao, and C. Davis: "Radiative Transfer Codes Applied to Hyperspectral Data for the Retrieval of Surface Reflectance", Proceedings of the 2nd EARSeL Workshop on Imaging Spectroscopy, Enschede, The Netherlands, 2000 (in press).

[Swayze 92] G. Swayze, R.N. Clark, F. Kruse, S. Sutley, and A. Gallagher: "Ground-Truthing AVIRIS Mineral Mapping at Cuprite, Nevada", Summaries of the Third Annual JPL Airborne Geoscience Workshop, Pasadena, California, U.S.A., 1992, JPL Publication 92-14, Vol. 1, pp. 47-49.

[Szeredi 00] T. Szeredi, K. Staenz, and R.A. Neville: "Automatic Endmember Selection: Part I Theory", *Remote Sensing of Environment*, 2000 (submitted).

[USGS 98] USGS: "Mineral map of Cuprite from AVIRS 1998 Data", http://speclab.cr.usgs.gov/cuprite98-low/cuplow+high.html.